



**HAL**  
open science

## Regeneration of an aged hydrodesulfurization catalyst : Conventional thermal vs non-thermal plasma technology

Hawraa Srour, Elodie Devers, Adrien Mekki-Berrada, Joumana Toufaily,  
Tayssir Hamieh, Catherine Batiot-Dupeyrat, Ludovic Pinard

### ► To cite this version:

Hawraa Srour, Elodie Devers, Adrien Mekki-Berrada, Joumana Toufaily, Tayssir Hamieh, et al.. Regeneration of an aged hydrodesulfurization catalyst : Conventional thermal vs non-thermal plasma technology. *Fuel*, 2021, 306, pp.121674. 10.1016/j.fuel.2021.121674 . hal-03597653

**HAL Id: hal-03597653**

**<https://ifp.hal.science/hal-03597653>**

Submitted on 22 Aug 2023

**HAL** is a multi-disciplinary open access archive for the deposit and dissemination of scientific research documents, whether they are published or not. The documents may come from teaching and research institutions in France or abroad, or from public or private research centers.

L'archive ouverte pluridisciplinaire **HAL**, est destinée au dépôt et à la diffusion de documents scientifiques de niveau recherche, publiés ou non, émanant des établissements d'enseignement et de recherche français ou étrangers, des laboratoires publics ou privés.



Distributed under a Creative Commons Attribution - NonCommercial 4.0 International License

# 1    **Regeneration of an Aged Hydrodesulfurization Catalyst:** 2    **Conventional Thermal vs Non-Thermal Plasma Technology**

3    Hawraa Srour <sup>1</sup>, Elodie Devers <sup>2</sup>, Adrien Mekki-Berrada <sup>2</sup>, Joumana Toufaily<sup>3</sup>, Tayssir Hamieh<sup>3</sup>,  
4    Catherine Batiot-Dupeyrat<sup>1</sup> and Ludovic Pinard <sup>1,\*</sup>

5    <sup>1</sup> Institut de Chimie des Milieux et Matériaux de Poitiers (IC2MP), UMR 7285 CNRS, 4 rue Michel  
6    Brunet, Bâtiment B27, TSA 51106, 86073 Poitiers Cedex 9 – France.

7    <sup>2</sup> IFP Energies nouvelles, Rond-point de l'échangeur de Solaize, BP 3, 69360 Solaize, France

8    <sup>3</sup> Laboratoire des matériaux, catalyse, environnement et méthodes analytiques (MCEMA), Université  
9    Libanaise, Liban

10

11    \* Corresponding authors:    ludovic.pinard@univ-poitiers.fr  
12       catherine.batiot.dupeyrat@univ-poitiers.fr

13

## 14    **Abstract**

15    This study compares the regeneration efficiency of an aged industrial  
16    hydrodesulfurization catalyst (CoMoP/Al<sub>2</sub>O<sub>3</sub>) by conventional and alternative routes:  
17    thermal oxidation versus non-thermal plasma technology (NTP). Spent, partially, and  
18    fully regenerated catalysts have been characterized by XRD, XPS, and toluene  
19    hydrogenation to measure hydrogenating activity. Complete regeneration of the HDS  
20    catalyst via NTP requires the heating of the dielectric barrier discharge plasma  
21    reactor. Total removal of coke is obtained from 250 °C by applying only 8.6 W/g<sub>catalyst</sub>,  
22    against 400 °C by conventional thermal treatment. The hydrogenation activity of the  
23    regenerated catalyst by NTP assisted by temperature is higher than that obtained by  
24    traditional thermal regeneration practiced industrially. Plasma treatment mitigates the  
25    oxide sintering but leads to the formation of cobalt oxide species preventing Co of  
26    fully playing its role as MoS<sub>2</sub> slabs promoter. HDS catalyst regeneration using non-  
27    thermal plasma assisted by low temperature appears as a promising alternative to  
28    thermal combustion.

29

30    Keywords: HDS catalyst, thermal regeneration, non-thermal plasma, coke

31

32

33

34

35

36

37

38

39

40

41

## 42 **1. Introduction**

43 It is well known that air pollution is a severe environmental problem. The combustion  
44 of organosulfur and organonitrogen compounds present in feedstocks are  
45 responsible for the generation of atmospheric air pollutants such as SO<sub>x</sub>, NO<sub>x</sub>, and  
46 particulate matter. Consequently, hydrotreatment processes are required to remove  
47 such compounds before conversion into gas oil in refinery units. The sulfur content  
48 must be less than 10 ppm in commercial on-road gas oils [1].

49 The hydrodesulfurization (HDS) process is used to remove sulfur-containing  
50 compounds from gasoline and diesel fuels. The most widely employed catalyst for  
51 the hydrodesulfurization process is cobalt-molybdenum supported on alumina [2].  
52 The industrial catalysts are relatively robust; for example, typical commercial HDS  
53 catalysts have a lifetime of 2–4 years in industrial applications [3]. However,  
54 deactivation is still a problem of great concern. The three typical causes of  
55 deactivation of hydroprocessing catalysts are coke, sintering, and contamination.

56 Coke deposition is one of the main reasons for the deactivation. Koh [4] identified two  
57 types of carbonaceous species deposited on the CoMo/Al<sub>2</sub>O<sub>3</sub> catalyst in the HDS of  
58 dibenzothiophene (DBT): the reactive and the refractory species. The authors  
59 indicated that the refractory deposit, or hard coke, was a significant contributor to the  
60 deactivation. The alumina support is assumed to be rapidly covered by coke, while  
61 the active sites remain protected by their high hydrogenation activity [5].

62 The coke can be eliminated by regeneration, the ex-situ method being the rule  
63 nowadays for better performance recovery. Regeneration consists of controlled  
64 oxidation, which removes coke and converts sulfides back to oxides. Traditionally,  
65 the most widely used method for catalyst activity recovery is oxidative regeneration  
66 using diluted-air. The experimental conditions used were optimized and particularly in  
67 terms of temperature, as it must not exceed 500 °C to limit the formation of  
68 crystallized species such as CoMoO<sub>4</sub> or CoAl<sub>2</sub>O<sub>4</sub> [6]. However, the presence of these  
69 phases is frequently observed after the regeneration step, while they are known to be  
70 refractory to sulfidation, influencing the HDS activity negatively [7].

71 The more recent works on catalyst regeneration are dealing with rejuvenation, i.e.  
72 reactivation using organic additives after thermic regeneration [8-9]. Recent works

73 start to deal with global cycle life of catalyst which of course include regeneration [10-  
74 11]

75 Consequently, there are needs to propose new strategies to perform catalyst  
76 regeneration. Among alternative processes and as indicated in the paper: “The 2020  
77 plasma catalysis roadmap” [12], non-thermal plasma treatment appears as an  
78 effective technique for removing coke from various spent catalysts [13].

79 Under plasma containing oxygen, active species are produced, such as  $O_2^+$ ,  $O^-$ ,  $O_2^-$   
80 and  $O_3^-$  [14], able to oxidize heavy molecules (graphitic or polyaromatic coke  
81 molecules [15] at atmospheric pressure and room temperature. The use of a  
82 Dielectric Barrier Discharge (DBD) plasma eliminated solid carbon of a Pt-Sn/ $Al_2O_3$   
83 catalyst using a pin to plate DBD plasma geometry [16]. A similar system was  
84 successfully used for the complete regeneration of coked zeolite [17, 18] and an  
85 industrial aged hydrotreating catalyst [19]. A coaxial DBD reactor is more suitable for  
86 an application of industrial scale. This configuration was also employed to regenerate  
87 a coked HFAU zeolite, and a kinetic study was performed, exhibiting the formation of  
88 carboxylic compounds as intermediates to  $CO_2$  [205].

89 The efficiency of this alternative regeneration process depends strongly on the nature  
90 of coke. Higher character polycyclic compounds of the coke, lower their reactivity  
91 relative to the short-lived oxygenated species [20].

92 In this study, the regeneration of an aged industrial hydrodesulfurization catalyst was  
93 investigated in a fixed bed DBD plasma reactor. The plasma treatment was  
94 performed in the temperature range 70 to 300 °C since it has been shown that  
95 plasma is able to regenerate catalysts at temperatures lower than those of typical  
96 thermal regeneration [13]. The efficiency of the conventional and plasma routes will  
97 be compared in terms of recovery of toluene hydrogenation activity.

## 98 **2. Experimental**

99 The catalyst studied is a used industrial phosphorus-doped CoMoP/ $Al_2O_3$   
100 hydrotreatment catalyst, with the following mass composition 20.5%,  $MoO_3$ , 4.0%  
101 CoO, 5.2%  $P_2O_5$ . The surface area determined by the BET method is 145  $m^2/g$ .

102 . It was recovered from a hydrodesulfurization process after two years on stream.  
103 Before any treatment, the catalyst was washed with toluene in a Soxhlet type device  
104 to extract the coke portion soluble in toluene (soft coke). The spent catalyst is

105 refluxed at 250 °C for 7 hours. The catalyst is then placed in a primary vacuum oven  
106 (30 mbar) at 150 °C for 3 hours. Before regeneration, spent catalysts were crushed  
107 and sieved to obtain homogeneous particles (0.1-0.2 mm).

108 The regeneration reactor is a cylindrical dielectric barrier discharge plasma reactor  
109 (DBD reactor) located in a furnace (**Figure 1** The temperature of the oven was  
110 regulated with a thermocouple at the inner wall of the oven. The Non-Thermal  
111 Plasma (NTP) reactor is made of an alumina tube of 6 mm of outer diameter.  
112 Alumina ceramic reactors were already used in various plasma applications due to  
113 their well-known long life, chemical stability, high hardness, temperature resistance  
114 [21-23]. The outer electrode, a copper sheet, is attached to the reactor by a special  
115 conductive glue. The inner electrode, a stainless steel rod (1.16 mm), is centred  
116 inside the reactor by a Teflon circle piece. Quartz wool folded around the inner  
117 electrode just under the plasma zone level holds the catalyst. The inner diameter of  
118 the reactor is 4 mm this corresponds to a gap of 1.42 mm. The plasma discharge is  
119 maintained in the zone between the two electrodes along 20 mm in length. The  
120 electrodes were connected to a high voltage (HV) sinusoidal generator. A low-  
121 frequency generator (GBF) from TTI® model TG1010A was coupled to a signal  
122 amplifier from TREK® model 30 / 20A. The signal delivered by the GBF is sinusoidal.  
123 The amplifier increases the voltage supplied by the GBF (x 3000 peak to peak),  
124 allowing it to work at high voltages. Power is supplied by coupling the low frequency  
125 generator and the amplifier. The high voltage is transmitted to the central electrode,  
126 located in the reactor, through a long shielded cable. The deposited power was  
127 measured by Q-U Lissajous method [24].

128 Non-thermal plasma regeneration (**NTP-R**) was carried out with gas feed composed  
129 of 20 vol% O<sub>2</sub> in He. Helium promotes energy transfer through the Penning effect to  
130 increase the concentration of active oxygen species (O<sub>2</sub><sup>+</sup>, O<sup>-</sup>, O<sub>2</sub><sup>-</sup> and O<sub>3</sub>) in the gas  
131 phase [17-20]. The GHSV through the plasma reactor, calculated at 20 °C and 1 atm,  
132 was fixed to 6 000 h<sup>-1</sup>, and the catalyst mass used is 350 mg. **NTP-R** was carried out  
133 at an input temperature of 70, 150, 200, and 300 °C. The catalytic bed temperature  
134 was measured with optic fiber in contact catalyst (Figure 1), and it was observed that  
135 it reaches approximately 100 °C when 70°C was applied and was not significantly  
136 modified for 150 °C and higher input temperatures because to the regulation of oven  
137 which takes account additional heat from NTP

138 The gas flow composition after the reactor was determined by on-line gas  
139 chromatographic analysis (Micro GC Varian CP 4900) equipped with a TCD detector,  
140 using a "CO<sub>x</sub> column." Only CO<sub>2</sub> and CO are measured, the organic molecules  
141 (VOC) and water are trapped upstream of the  $\mu$ GC in order to protect it.

142 Thermal regeneration was carried out in the DBD plasma reactor (**TR<sub>DBD</sub> reactor**)  
143 through a fixed bed in the same operating conditions (20% vol O<sub>2</sub>, GHSV= 6000 h<sup>-1</sup>,  
144  $m_{\text{catalyst}} = 350$  mg) as these used for the plasma regeneration, except that the  
145 generator is turned off. The temperature of the oven is fixed at 320, 350, 380, and  
146 450 °C.

147 Optimized thermal regeneration (**O-TR**) consists of controlled combustion by injecting  
148 oxygen through a solenoid valve. The spent catalyst is placed in a vertical furnace  
149 under nitrogen flow (6L.h<sup>-1</sup>.g<sup>-1</sup>). The heating ramp is set at 5°C/min until 250 °C  $\pm$ 10  
150 °C is reached. The oxygen flow rate is then adjusted to inject 5% vol. of oxygen. If  
151 the exothermicity exceeds 2 °C, the solenoid valve closes automatically, and the  
152 catalyst is flushed with nitrogen only. The oxygen injection only resumes when the  
153 temperature has dropped to 250 °C under 5% vol., 10% vol. Oxygen is injected, and  
154 when there is no more exothermicity at 250 °C under this condition, the oxygen feed  
155 is stopped. The catalyst is heated under nitrogen to the next temperature (maximum  
156 50 °C) at the desired temperature; the oxygen injections start again under the same  
157 conditions as before. The catalyst is regenerated at different temperatures between  
158 300 and 450 °C.

159 The amount of carbon and sulfur of the spent, partially, and fully regenerated  
160 catalysts was measured using a C.E. Instruments NA2100 PROTEIN  
161 elementary analyser.

162 X-ray diffraction patterns of the fresh, spent, and partially regenerated catalysts  
163 were recorded using a Malvern Panlytical®, Empyrean model diffractometer  
164 operating with Cu K $\alpha$ 1 (radiation ( $\lambda=0.15406$  nm ) in the range of 10° <2 $\theta$  < 80°  
165 with a step of 0.04° using a zero background holder with a 32 mm diameter.

166 XPS characterizations were made on the catalysts after the toluene  
167 hydrogenation catalytic test (see more below). The XPS sampling of the

168 catalysts was performed in a glove box under an argon atmosphere to prevent  
169 the partial reoxidation of MoS<sub>2</sub> nanocrystallites. The samples were crushed  
170 and pressed onto an indium foil on the sample holder and moved to the  
171 introduction chamber of the XPS spectrometer. The XPS spectra were  
172 recorded on a Kratos Axis Supra instrument assembled with an aluminum  
173 monochromator source (1486.6 eV) and a hemispherical analyzer functioning  
174 at fixed pass energy of 20 eV. The measurements were made at 20 °C in steps  
175 of 0.1 eV for cobalt, 0.1 eV for sulfur, and 0.1 eV for molybdenum, and at a  
176 pressure lower than 10-12 bar in the sample analysis chamber. C 1s peak at  
177 284.6 eV was used as an internal standard for binding energy calibration. The  
178 curves were integrated by applying a Shirley type baseline. The collected  
179 spectra were analyzed by using Plug Im! software. The decomposition of the S  
180 2p, Mo 3d and Co 2p signals was performed using the appropriate oxide and  
181 sulfided references as supported monometallic catalysts and according to the  
182 methods already described, and particularly to quantify the promoted CoMoS  
183 phase [25-26]. The Mo 3d spectra of sulfided catalysts were first decomposed  
184 (**Figure 2a**). Three different oxidation degrees of molybdenum were found:  
185 Mo<sup>+VI</sup> (232.2 eV), Mo<sup>+V</sup> (MoS<sub>x</sub>O<sub>y</sub>, 229.8 eV), and Mo<sup>+IV</sup> (MoS<sub>2</sub>, 228.7 eV). They  
186 were, respectively, attributed to the oxide, oxysulfide, and sulfide phases. We  
187 then fixed a gap of 549.95 eV between MoS<sub>2</sub> and CoMoS and 0.49 eV  
188 between CoMoS and Co<sub>9</sub>S<sub>8</sub>, the third contribution being the cobalt oxide,  
189 which has to be integrated to correctly fit the spectrum (+/-0.5 eV). (**Figure 2b**)

190 Similarly, the decomposition of the S 2p reveals three components,  
191 corresponding to three local environments: S<sub>Sulf</sub> (fully sulfided), SO<sub>x</sub> (oxysulfide  
192 species), and S<sub>Sulfates</sub> (fully oxidized) ). The fully oxidized form of S detected  
193 here is due to the partial exposure of the sample to air while transferring it to  
194 the XPS sampling chamber

195 The XPS decomposition led to the quantification of the relative amount of each  
196 species as follows:

$$197 \quad [j] = \frac{A_j/S_j}{\sum_{i=1}^n A_i/S_i} \times 100 \quad (\text{Eq.1})$$

198 where  $A_i$  is the measured area of each species,  $S_i$  is the sensitivity factor for the  
199 atom related to the species  $i$ .  $[j]$  is the relative amounts of the various species.

200 The molybdenum sulfidation rate (SR) is calculated by assuming that all Mo is  
 201 transformed into MoS<sub>2</sub>. Mo SR is defined as

$$202 \quad MoSR = \frac{[MoS_2]}{[Mo]} \times 100 \quad (\text{Eq.2})$$

203 The ratio of Co/Mo in the sheets (Co/Mo)<sub>sheet</sub> is calculated as:

$$204 \quad \left(\frac{Co}{Mo}\right)_{sheet} = \frac{[CoMoS]}{[MoS_2]} \quad (\text{Eq.3})$$

205

206 The impact of regeneration on catalytic performances was evaluated in toluene  
 207 hydrogenation reaction using a fixed bed unit reactor Flowrence rom Avantium. This  
 208 reaction is considered as a model reaction for HDS catalyst since the most refractory  
 209 species such as 4,6DMDBT react according to two main paths, the direct  
 210 desulfurization (DDS) and the hydrogen path (HYD). This last one need the  
 211 hydrogenation of aromatic rings before the rupture of the C-S bond and is the main  
 212 path as described in Pérot, G. et al. [27]. As a consequence, using Toluene  
 213 hydrogenation in presence of DMDS is a suitable model reaction. The main products  
 214 are Methylcyclohexane, Ethylcyclopentane and Dimethylcyclopentane.

215 The reactor was filled with 450 μL of the catalyst diluted in Zirblast®. The feed was  
 216 composed of dimethyldisulfide (DMDS, 5.8 wt%) and toluene (20 wt%) in  
 217 cyclohexane (74.2 wt%). The hydrogen to feed ratio (H<sub>2</sub>/HC) was kept at 450 NL.L<sup>-1</sup>  
 218 during the test and the in-situ presulfidation step, which was performed at a liquid  
 219 hourly space velocity (LHSV) of 4 h<sup>-1</sup> with a total pressure of 60 bar for 2 h. The  
 220 temperature was increased from room temperature to 350 °C with a ramp of 2°C min<sup>-1</sup>.  
 221 After this presulfidation step, LHSV was turned down to 2 h<sup>-1</sup>. The liquid products of  
 222 the reaction at different temperatures were analyzed by gas chromatography using a  
 223 DB1 column. The first-order rate constant (k, h<sup>-1</sup>) was calculated by the following  
 224 expression:

$$225 \quad k'_{regenerated\ catalyst} = LHSV * \ln\left(\frac{1}{1-x}\right), LHSV = \frac{\text{flow rate of the liquid feed}}{\text{volume of the catalyst}} \quad (\text{Eq. 4})$$

226

227 x is the percentage conversion of toluene (HYD) in the feed. LHSV is the liquid hourly  
 228 space velocity (h<sup>-1</sup>). All the catalytic results will then be expressed as the Relative  
 229 Volumic Activity *RVA(HYD)*, the industrial regenerated catalyst activity being the  
 230 reference, according to the following equation :

$$231 \quad RVA(HYD) = \frac{k'_{regenerated\ catalyst}}{k'_{indus\ rege\ catalyst\ (internal\ reference)}} \quad (\text{Eq. 5})$$

232

### 233 3. Results and discussion

#### 234 3.1. Conventional regeneration method ( $TR_{DBD}$ reactor)

235 The carbon and sulfur contents on the spent catalyst, determined by elementary  
236 analysis, are 13.0 and 8.8 wt. %, respectively. Sulfur derives largely from the  
237 remaining sulfur phase, i.e.,  $CoMoS$ ,  $MoS_2$ ,  $Co_9S_8$  [28].

238 The thermal regeneration of the spent catalyst was carried out under  $100\text{ mL}\cdot\text{min}^{-1}$   
239 airflow at a range of temperature 320-450 °C. **Figure 3** shows the cumulative yields  
240 of  $CO_2$  and  $CO$  as a function of the treatment time at different temperatures and the  
241 relative C and S removals measured by elemental analysis after 1 hour. Regardless  
242 of the protocols used for thermal regeneration: fixed bed ( $TR_{DBD}$  reactor) reactor, with  
243 (**O-TR**) or without isothermal conditions, coke and sulfur removal rates are similar.

244 Cumulated yields into  $CO_2$  measured for  $TR_{DBD}$  reactor exhibit a rapid and high  
245 increase as soon as the fixed temperature is reached (corresponding to point 0),  
246 exhibiting a plateau after 20 minutes of thermal treatment at 380 and 450 °C while  
247 the yield into  $CO_x$  still increases until 60 minutes at the lowest temperature, 320 and  
248 350 °C. (**Figure 3a**). It is probably due to the reaction's exothermicity, which  
249 significantly increases the temperature into the catalytic bed. Comparing the yield into  
250  $CO_x$  with C removal determined after regeneration (**Figure 3b**), it can be observed  
251 that the carbon balance is incomplete, whatever the temperature. The amount of C  
252 removed as  $CO_x$  reaches 85 % at 450 °C, proving that heavy coke molecules are not  
253 selective into  $CO_x$ . This partial selectivity means that one part of the coke molecules  
254 is oxidized into desorbed products that are not detected, assumed as intermediate  
255 products [18-20].

256 It is confirmed that it is easier to remove sulfur than carbon under thermal treatments  
257 [5]. Probably, the location of a large portion of sulfur on the metallic phase as  $MoS_2$   
258 slabs facilitates its oxidation. A significant quantity (75 %) of sulfur was eliminated at  
259 the lower temperature, 320 °C.

260 **Figure 4** shows XRD patterns of the spent catalyst and the thermally treated samples  
261 at different temperatures. For the spent catalyst,  $Al_2O_3$  Bragg peaks are recognized

262 at  $2\theta = 33.4^\circ, 37^\circ, 39.5^\circ, 46.1^\circ, 66.7^\circ$  and  $\text{MoS}_2$  at  $59^\circ$ . The TEM Micrograph of the  
263 spent catalyst before treatment (**Figure 5**) displays black thread-like fringes, which  
264 corresponds to the structure of molybdenum disulfide  $\text{MoS}_2$  slabs [5]. The  $\text{MoS}_2$   
265 slabs are randomly oriented and homogeneous distributed on the alumina support.  
266 Regardless of the thermal treatment,  $\text{Al}_2\text{O}_3$  Bragg peaks are always detected.  
267 However, the patterns exhibit high noise leading to undefined signals. Starting from  
268  $300^\circ\text{C}$ , the Bragg peaks assigned to  $\text{MoS}_2$  disappeared, in coherence with S  
269 removal. At high temperature,  $500^\circ\text{C}$ , a new range of peaks appeared between  $2\theta =$   
270  $26.5^\circ$  and  $39.5^\circ$ , assigned to  $\text{CoMoO}_4$ ; which are species refractory to sulfidation  
271 [29]. This is paired with the sintering effect and could be attributed to the aggregates  
272 (Al, O, P, Co, Mo) observed by TEM at  $500^\circ\text{C}$  **Figure 5**).

273

### 274 **3.2. Regeneration by non-thermal plasma (NTP-R)**

275 The coked catalyst was treated by plasma in the temperature range:  $70\text{-}300^\circ\text{C}$ .  
276 Experiments were performed to keep the frequency at 2 kHz, while the applied  
277 voltage varied from 7 to 12kV. As expected, the deposited power increases with the  
278 applied voltage regardless of the temperature (**Figure 6a**). With the increase in  
279 temperature, a shift in the breakdown voltage to lower values is observed. At  $70^\circ\text{C}$ ,  
280 the plasma appears from 9 kV, while only 6.5 kV is enough at  $300^\circ\text{C}$ . Otherwise, to  
281 obtain an applied power of 5 W, an input voltage of 11.6 kV is needed at  $70^\circ\text{C}$ , while  
282 7.2 kV at  $300^\circ\text{C}$ . The power depends on both the input voltage and the temperature  
283 (see Lissajous Figures in SI). Higher the temperature, lower the gas density, and  
284 higher the power [30].

285 As a corresponding sum up of these operational results, **Figure 6b** allows selecting  
286 the suitable operating conditions (U, T, P) to progress the study of iso-power plots,  
287 making it possible to know the value of input voltage needed to deposit an applied  
288 power ( $P_A$ ) at a specific temperature. Therefore in this article, the results will be  
289 measured using a chosen  $P_A$ .

290 **Figure 7** shows the light-off curves of C and S removals, the yield into  $\text{CO}_x$ , and  
291 carbon balance as a function of the temperature under plasma-assisted by  
292 temperature (**NTP-R**) at different applied power ( $P_A$ ). This data is compared with the

293 relative thermal treatment evolutions. With **NTP-R**, up to 150 °C, there is no  
294 significant modification of the C removal by temperature (**Figure 7a**) with C removal  
295 depending only on the amount of active species generated ( $P_A$ ). From 200 °C, there  
296 is a rapid increase in C removal, which becomes total at 300 °C, regardless of the  $P_A$   
297 (**Figure 7a**). By opposition, S removal (**Figure 7b**) appears more sensitive to  
298 temperature, with a constant increase starting from low temperatures. These results  
299 show that the regeneration of HDS catalysts via NTP need to be temperature  
300 assisted. At a fixed temperature, both C and S removals are proportional to the  $P_A$   
301 (**Figures 8a and 8b**). In opposition to thermal treatment plasma promotes easier C  
302 removal than S removal at a lower temperature (**Figures 7 and 8**). Indeed, the most  
303 significant benefit of **NTP-R** is the lower temperature needed to reach total C and S  
304 removals. A gap of  $\Delta T=100$  °C at a range of  $P_A$  of 2W-6W, and  $\Delta T= 200$  °C at a  $P_A$  of  
305 7W were observed (**Figures. 7a and 7b**).

306 Regardless of temperature and  $P_A$ , the yield of  $CO_x$  is always lower than C removal  
307 (**Figures 7c and 8c**). This difference indicates that C balance (**Figure 6d**) for **NTP-R**  
308 is incomplete as observed with thermal treatment. It was observed that C balance  
309 depends mainly on the applied temperature (**Figure 7d**), the higher the temperature,  
310 the higher the carbon balance. Unfortunately, XRD evidences traces of  $CoMoO_4$   
311 formation even at 200°C under plasma discharge (**Figure 4**).

312 From the collected data, it is possible to calculate apparent activation energy ( $E_a$ )  
313 using Arrhenius law (**Figures 9a and 9b**). The  $-\ln(\text{C removal})$  and  $-\ln(\text{S removal})$   
314 plots exhibit straight lines with a proportional linear increase as a function of  $1/T$  at  
315 the different  $P_A$ . The equivalent slopes, which are equal to  $(-E_a/R)$ , increase with the  
316 decrease in the  $P_A$  in **NTP-R** treatments, with a higher slope in the case of thermal  
317 treatment. **Figure 10** reports the  $E_a$  of C and S removals as a function of the  $P_A$  for  
318 **NTP-R** compared to the thermal treatment. It appears that with thermal treatment, the  
319  $E_a$  is four times lower in the case of S removal with a value of 15  $\text{kJ}\cdot\text{mol}^{-1}$ . The  
320 decomposition of  $MoS_2$  slabs requires lower activation energy than coke oxidation  
321 reaction ( $E_a= 60 \text{ kJ}\cdot\text{mol}^{-1}$ ). The most important is the comparison with **NTP-R**, in  
322 which, there is a large drop in  $E_a$  of C removal to 25  $\text{kJ}\cdot\text{mol}^{-1}$  at only a  $P_A$  of 2W, while  
323 it is not the case for S where  $E_a$  at 2W is similar to thermal. As a function of  $P_A$  of  
324 **NTP-R**, for both C and S, there is no significant difference as recognized in thermal,  
325 and  $E_a$  exhibits a continuous decrease as a function of  $P_A$  reaching values lower than

326 10 kJ.mol<sup>-1</sup> at higher P<sub>A</sub>. It highlighted that the mechanism involved in C and S  
327 removals seems to be different between thermal treatment and **NTP-R**

328 The apparent activation energy for thermal regeneration is similar to that measured  
329 for the catalytic oxidation of light alkanes and aromatics (54-75 kJ.mol<sup>-1</sup>) [31-34], and  
330 much lower than that of their pyrolysis, which occurs by C-C bond breaking (E<sub>a</sub> > 160  
331 kJ mol<sup>-1</sup>) [32]. Moreover, E<sub>a</sub> for NTP operating at moderate temperature is  
332 comparable to those measured for the attack of the oxygen radical on *n*-alkanes [34]:



334 These values suggest that the NTP oxidation mechanism follows a radical  
335 mechanism and initiates by breaking the C-H bond. The oxidation mechanism of  
336 thermal regeneration is different than the one occurring during NTP. **Figure**  
337 **11a** supports this assumption, since it reports the product selectivity for both  
338 treatments by the plots of the yields into CO<sub>x</sub> as a function of the coke conversion. By  
339 extrapolating the beginnings of the plots, CO<sub>x</sub> seems to be the primary product in  
340 thermal treatment, while in **NTP-R** it is a secondary product. **Figure 11b** shows the  
341 molar ratio CO<sub>2</sub>/CO versus the applied temperature at different PA. At low  
342 temperatures (<200 °C), the selectivity into CO<sub>2</sub> is much higher than CO, as indicated  
343 by the high ratio that reaches 25 mol/mol at 70 °C. While at high temperatures (> 200  
344 °C), the molar ratio decreases, then becomes almost constant at 5 mol/mol  
345 regardless of the PA and equal to that of the thermal treatment.

346 XRD evidences CoMoO<sub>4</sub> formation even at 200°C under plasma discharge .

### 347 **3.3. Comparison of the performances of the industrial (I-TR) and optimised** 348 **thermal (O-TR) and to NTP regeneration (NTP-R) routes.**

349 **Figure 12** compares the relative volumic activity (RVA) in toluene hydrogenation of  
350 regenerated catalyst by optimized thermal and NTP technologies; with the industrial  
351 regenerated catalyst activity being used as the reference (data supplied by IFPEN).  
352 Industrial, optimized thermal and non-thermal plasma regeneration are named **IT-R**,  
353 **OT-R**, and **NTP-R**, respectively. (**Table 1**) It is worth mentioning that results obtained  
354 on the NTP reactor (turn-off) and at the lab scale at IFPEN (OT-R) are similar (**Figure**  
355 **3b**).

356 The Regeneration in an industrial unit eliminates coke but leads to undesirable  
357 CoMoO<sub>4</sub> species' formation due to hot spots. RVA increases in proportion to coke  
358 removal, suggesting that coke is rather located on the hydrogenating sites (MoS<sub>2</sub>)  
359 than on the support (Al<sub>2</sub>O<sub>3</sub>). Yet, thermal regeneration, performed with different  
360 temperature plateaus, limits and even prevents at a lower temperature the formation  
361 of CoMoO<sub>4</sub>.

362 This regeneration protocol improves the hydrogenation activity by 1.4 compared to  
363 the conventional industrial thermal regeneration. A substantial benefit (x 1.25) is  
364 obtained after **NTP-R** at 300 °C. Regardless of the applied power (3, 4, and 7 W) and  
365 the temperature used (200 and 300 °C), RVA after plasma regeneration at low  
366 temperature is also proportional to the coke elimination. The lower recovery efficiency  
367 of the hydrogenation activity by the **NTP-R** is not merely due to the presence of  
368 CoMoO<sub>4</sub>. But probably to the modifications of the catalyst surface.

369 XPS characterizations were performed on the sulfide catalyst after toluene  
370 hydrogenation (**Figure 2**). **Table 1** compares the sulfidation rate and metal  
371 distribution with different coordination (Co Ox, S-Co, CoMoS) over catalysts  
372 regenerated using industrial and optimized thermal conditions and NTP at low  
373 temperatures. The NTP treatment leads to a slight increase in the molar ratios Mo/Al,  
374 suggesting a somewhat higher MoS<sub>2</sub> dispersion after non-thermal plasma  
375 regeneration than upon the optimized thermal treatment.

376 The advantage of NTP regeneration over thermal is the mitigation of oxide sintering.  
377 The ratios of (Co/Mo) sheets are similar on the catalysts after IT-R and **NTP-R**, but  
378 lower than after optimized thermal regeneration. The thermal regeneration  
379 optimization leads to better promotion of MoS<sub>2</sub> slabs by cobalt, consistent with a  
380 slightly higher % of CoMoS. The regeneration route has thus a real impact on the  
381 distribution of Co species after sulfiding treatment. The proportion of Co coordinated  
382 to a sulfur (Co-S) is significantly higher after **NTP-R** than after OT-R. Thus, cobalt no  
383 longer plays its role as a promoter, which harms the hydrogenation activity.

384

## 385 **Conclusion**

386 The regeneration of the hydrodesulfurization catalyst is a challenge of great concern  
387 for oil refineries. The coke removal from an aged CoMoP/Al<sub>2</sub>O<sub>3</sub> HDS industrial  
388 catalyst was studied using a non-thermal plasma reactor with coaxial geometry. NTP  
389 regeneration was carried out at a temperature ranging from 70 and 300 °C by  
390 applying power between 2 and 7W.

391 Complete removal of sulfur and coke is obtained under air from 400 °C but leads to  
392 the formation of undesirable species (CoMoO<sub>4</sub>), which yields to an irreversible  
393 deactivation of the HDS catalyst. The apparent activation energies on coke and sulfur  
394 removal are 60 and 15 kJ. mol<sup>-1</sup>, respectively.

395 At low temperature (< 150 °C and under non-thermal plasma (NTP) conditions), the  
396 oxidation efficiency of coke and sulfur is proportional to the power applied, but their  
397 removals remain partial. Complete regeneration of the catalyst requires the heating of  
398 the NTP reactor. Thus, the total elimination of sulfur and coke is obtained from 250  
399 °C by applying only 3 W power. The apparent activation energy for coke removal is  
400 divided by more than three and becomes close to that encountered for the oxidation  
401 of hydrocarbon molecules by radical oxygen.

402 However, XRD evidences CoMoO<sub>4</sub> formation even at 200°C under plasma discharge.  
403 Catalytic performances and XPS characterization suggest that the modification of  
404 catalyst surface with the formation of new oxidic species other than CoMoO<sub>4</sub> is  
405 responsible for a lower quantity of CoMoS phase after plasma regeneration leading  
406 to the lower recovery efficiency of the NTP treated catalyst when compared to  
407 optimized isothermal oxidation (OT-R). Despite the presence of CoMoO<sub>4</sub> and species  
408 of oxides preventing the cobalt from entirely playing its role as a promoter, the  
409 hydrogenation activity of regenerated HDS catalyst is higher than that obtained by  
410 conventional thermal regeneration in an industrial unit.

411 Non-thermal plasma regeneration is an alternative to the thermal route but still needs  
412 to be improved to avoid the formation of hot spots or maintain Co's promoter  
413 role. The oxidation of the catalyst surface must be controlled by adjusting the oxygen  
414 concentration in the feed gas, as in thermal regeneration optimization. Moreover, an  
415 optimization of the regeneration conditions (frequency variation, nature of the  
416 electrical signal, regeneration by sequences, etc.) should make it possible to achieve

417 the same performances as those obtained with optimized thermal regeneration.  
418 Moreover, the use of NTP for catalyst rejuvenation could also be considered.

419  
420 **Acknowledgments:** The authors gratefully acknowledge IFPEN for the financial  
421 support. Hawraa Srour thanks the Lebanese University and IC2MP for the PhD grant.  
422 The authors acknowledge financial support from the European Union (ERDF) and  
423 "Région Nouvelle Aquitaine". The authors would be grateful to O. Delpoux and L.  
424 Lemaitre for the XPS analysis, S. Lopez for technical support in catalyst preparation  
425 and regeneration.

426  
427 **References**

- 428 [1] V. Rabarihoela-Rakotovao, F. Diehl, S. Brunet, *Catal. Lett.*, 129 (2009) 50-60.  
429 [2] J.A. Rob Van Veen, *Catal. Today*, 292 (2017) 2-25.  
430 [3] C.H. Bartholomew, R.C. Reuel, *Chem. Eng.*, 24 (1985) 56-61.  
431 [4] J. H. Koh, J. J. Lee, H. Kim, A. Cho et S. H. Moon, *Appl. Catal. B: Environ.*, 86  
432 (2009) 176–181.  
433 [5] B. Guichard, M. Roy-Auberger, C. Pichon, *Appl. Catal. A*, 367 (2009) 9-22.  
434 [6] Y. Yoshimura, T. Sato, H. Shimada, N. Matsubayashi, *Energy & Fuels*, 8  
435 (1994) 435-445.  
436 [7] N.-Q. Bui, C. Geantet, G. Berhault, *J. Catal.*, 330 (2015) 374-386.  
437 [8] A. Pimerzin, A. Roganov, A. Mozhaev, K. Maslakov, P. Nikulshin, A. Pimerzin  
438 *Fuel Processing Technology* 173 (2018) 56–65.  
439 [9] N.-Q. Bui, C. Geantet, G. Berhault, *Applied Catalysis A, General* 572 (2019)  
440 185–19.  
441 [10] Y. Liu, S. Lu, X. Yan, S. Gao, X. Cui, Z. Cui, *Journal of Cleaner Production*  
442 256 (2020) 120422  
443 [11] A. Pathak, M. Vinoba, R. Kothari, Richa, *Crit. Rev. Env. Sc. Tech.* 51 (2021) :  
444 1-43.  
445 [12] A. Bogaerts, X. Tu, C. Xhiteheas, G. Centi, L. Lefferts, O. Guaitella, F.  
446 Assolina-Jury, H.-H. Kim, A. B. Murphy, W. F. Schneider, T. Nozaki, J. C.  
447 Hicks, A. Rousseau, F. Thevenet, A. Khacef, M. Carreon, *J. Phys. D: Appl.*  
448 *Phys.* (2020) **53** 443001

- 449 [13] D.H. Lee, Y.H. Song, K.T. Kim, S.Jo, H. Kang, *Catal. Today*, 337 (2019) 15-  
450 27.
- 451 [14] B. Eliasson, M. Hirth, U. Kogleschatz, *J. Phys. D. Appl. Phys.*, 20 (1987) 1421-  
452 1437.
- 453 [15] Y. Fan, Y. Cai, X. Li, H. Yin, L. Chen, S. Liu, *J. Anal. Appl. Pyro*, 111 (2015)  
454 209-215.
- 455 [16] N. Hafez Khiabani, S. Fathi, B. Shokri, S. I. Hosseini, *Appl. Catal. A : Gen*, 493  
456 (2015) 8-16.
- 457 [17] L. Jia, Al Farouha, L. Pinard, S. Hedan, J. -D Comparot, A. Dufour, K. Ben  
458 Tayeb, H. Vezin, C. Batiot-Dupeyrat, *Appl. Catal. B: Env*, 219 (2017) 82-91.
- 459 [18] L. Pinard, N. Ayoub et C. Batiot-Dupeyrat, *Plasma Chem. and Plasma*  
460 *Process.*, 239-4 (2019) 929-936.
- 461 [19] H. Srour, A. Alnaboulsi, A. Astafan, E. Devers, J. Toufaily, T. Hamieh, L.  
462 Pinard, C. Batiot-Dupeyrat, *Catalysts*, 9 (2019) 783-800.
- 463 [20] A. Astafan, C. Batiot-Dupeyrat, L. Pinard, *J. Phys. Chem. C*, 123 (14) (2019)  
464 9168-9175.
- 465 [21] A. H. Khoja, M. Tahir et N. A. S. Amin, *Energy Conv. and Manag.*, 144 (2017)  
466 262–274.
- 467 [22] M. S. Gandhi , Y. S. Mok, *J. Env. Sci.*, 24(7) (2012) 1234–1239.
- 468 [23] S. K. Kundu, E. M. Kennedy, V. V. Gaikwad, T. S. Molloy, Bogdan Z.  
469 Dlugogorski, *Chem. Eng. J.*, 180 (2012) 178–189.
- 470 [24] M. Hołub, *Int. J. of Appl. Electromagnetics and Mechanics*, 39 (2012) 81–87.
- 471 [25] A. D. Gandubert, C. Legens, D. Guillaume, S. Rebours, E. Payen, *Oil Gas*  
472 *Sci.Technol.* 62 (2007) 79- 83.
- 473 [26] A. D. Gandubert, C. Legens, D. Guillaume, E. Payen, *Surf. Inter. Anal.* 38  
474 (2006) 206-209
- 475 [27] G. Perot, *Catal. Today* 86 (2003) 111-128.
- 476 [28] M. Marafi, A. Stanislaus , *Appl.Catal. A: Gen.*, 159 (1997) 259-267.
- 477 [29] P.D. Hopkins et B.L. Meyers, *Ind. Eng. Chem., Prod. Res. Dev.*, 3 (1983) 421-  
478 426.
- 479 [30] B. Pietruska, M. Heintze, *Catal. Today*, 90 (2004) 151-158.
- 480 [31] M. Aryada , F. Zaera, *Catal. Lett.*, 48 (1997) 173-183.
- 481 [32] T. F. Garetto, C. R. Aspetegua, *Appl Catal. B: Env.I*, 32 (2001) 83-94.
- 482 [33] A; Ristori, P. Dagaut, M. Cathonnet, *Combust Flame*, 125 (2001) 1128-1137.

483 [34] W. Mayer, L. Schieler, J. Phys Chem, 73 (1968) 2628-2631.

484

485

486

487

488

489

490

491

492

493

## Figure and table captions

- Table 1: Operating conditions of industrial and optimised thermal regeneration processes and non-thermal plasma at low temperature. Sulfidation rate and metals repartition by XPS over catalyst after toluene hydrogenation
- Figure 1: Dielectric barrier discharge plasma reactor.
- Figure 2: Deconvolution XPS spectra of MO (a), Co (b) and S (c) elements.
- Figure 3: (a) Cumulative yield into CO<sub>x</sub> as a function of time at different regeneration temperatures: 320, 350, 380, and 450 °C, and (b) the relative C and S removals after 64 minutes.
- Figure 4: XRD patterns of spent catalyst before (a) and after thermal regeneration at 200 (b), 300 (c) and 500°C (d), in blue after plasma treatment at 200°C with 7W.
- Figure 5: TEM images of spent catalyst before after thermal regeneration during 30minutes at 500 °C
- Figure 6: Impact of temperature on deposited power (P):  
(a) P at different temperatures: 70, 150, 200 and 300°C as a function of the applied voltage;  
(b) Applied voltage (U) required to obtain a deposited power of 3, 4, 5, 6 and 7W as a function of the temperature.
- Figure 7: Impact of temperature on the efficiency of non-thermal plasma on: (a,b) carbon and sulfur removal, (c) cumulated conversion to CO<sub>x</sub> (CO<sub>2</sub>+CO), (d) carbon balance and comparison with thermal regeneration (Full symbol). Results obtained after 1h regeneration at different applied powers (2, 3, 4, 5, 6 and 7W).
- Figure 8: Impact of applied power (P) on the efficiency of non-thermal plasma on (a,b) carbon and sulfur removal, (c) cumulated conversion to CO<sub>x</sub> (CO<sub>2</sub>+CO), (d) carbon balance. Results obtained after 1h regeneration at different temperatures: 70, 150, 200 and 300 °C.
- Figure 9: Temperature dependency of removal of carbon (a) and sulfur (b) and apparent activation energy (E<sub>a</sub>) as a function of the applied power; Results obtained after 1h regeneration.
- Figure 9: Temperature dependency of removal of carbon (a) and sulfur (b) as a function of the applied power; Results obtained after 1h regeneration.
- Figure 10: apparent activation energy (E<sub>a</sub>) as a function of the applied power; Results obtained after 1h regeneration.
- Figure 11: Selectivity of NTP process:  
(a) Cumulated yield into CO<sub>x</sub> as a function of coke conversion drawn from elementary analysis,  
(b) Molar ratio of CO<sub>2</sub>/CO at different applied power as a function of temperature.

Figure 12: Relative Volumic Activity of toluene hydrogenation (the industrial regenerated catalyst activity being the reference) of spent catalyst (●) and regenerated catalysts by IT-R (◆), O-TR (□) and NTP-R (△) processes.

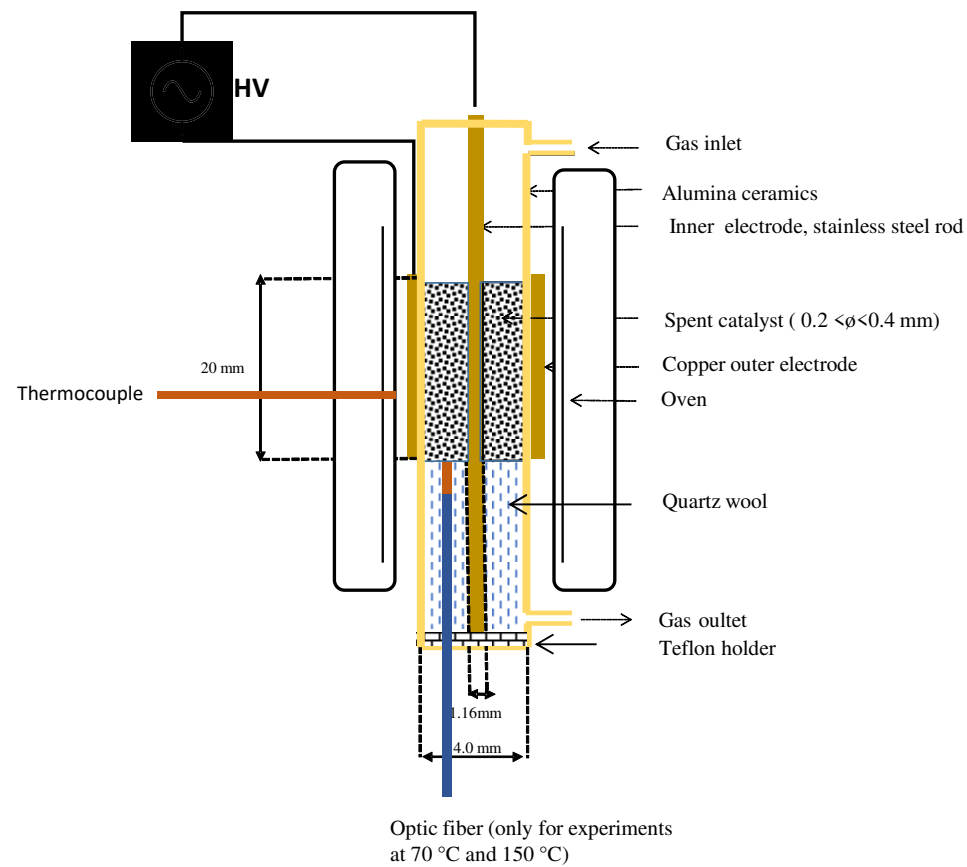
### Supporting Information

Fig. SI. 1 Lissajous figure for P=5W at 70, 150, 200 and 300°C during plasma treatment

**Table 1:** Operating conditions of industrial and optimised thermal regeneration processes and non-thermal plasma at low temperature. Sulfidation rate and metals repartition by XPS over catalyst after toluene hydrogenation.

Regeneration Mode	T (°C)	P (W)	Removal of (%)		Presence of CoMo <sub>4</sub> <sup>a</sup>	Mo/Al	Co/Al	(Co/Mo) <sub>sheet</sub> <sup>b</sup>	SR <sup>c</sup> (%)	Co repartition (rel.%)		
			C	S						Co <sup>2+</sup>	Co-S	CoMoS
I-TR	450		100	94.8	+++	0.31	0.08	0.25	73.3	36.2	21	43
O-TR	300		7.4	87.8		0.28	0.08	0.31	78.4	32.6	18	50
	320		56.0	94.6	Traces	0.33	0.10	0.31	76.6	34.4	16	50
	350		81.6	99.0	+	0.30	0.08	0.30	76.7	34.9	14	51
	450		99.6	100	+	0.37	0.08	0.29	75.5	40.6	12	48
NTP-R	200	4	54.2	66.2	Traces	0.37	0.11	0.31	77.8	28.0	24	48
	200	7	99.9	99.9	+	0.34	0.09	0.26	79.4	29.9	23	47
	300	3	98.8	97.9	+	0.34	0.09	0.24	78.1	32.6	25	43

<sup>a</sup> detected by XRD, <sup>b</sup> Co/Mo in the sheets calculated according to Eq. 3,, <sup>c</sup>Sulfitation rate calculated according to Eq. 2



**Figure 1:** Dielectric barrier discharge plasma reactor

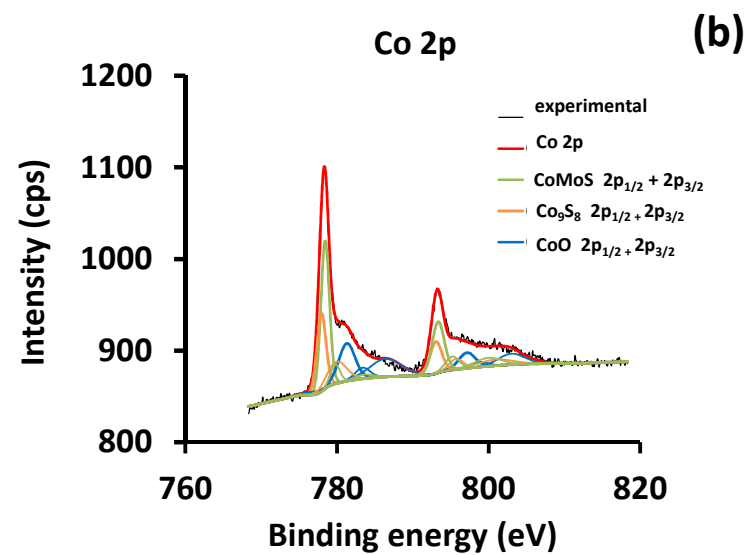
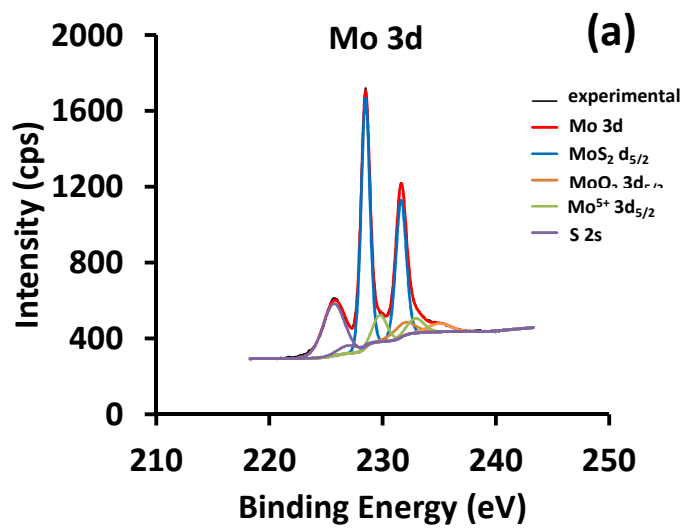


**Figure 2:** XPS spectra of after toluene hydrogenation: cobalt and molybdenum elements.

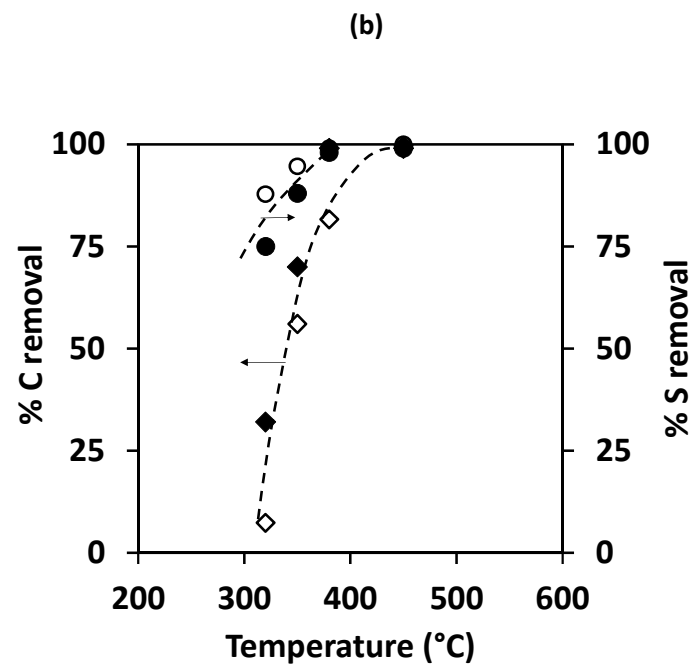
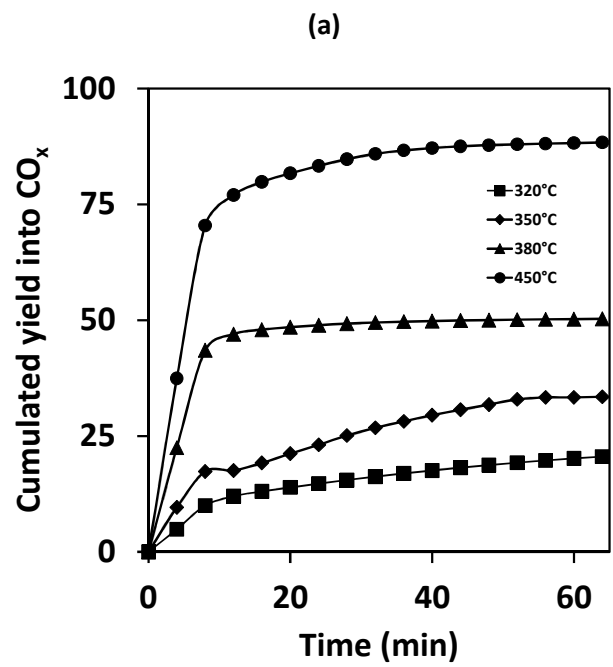


**Figure 3:** (a) Cumulative yield into  $\text{CO}_x$  as a function of time at different regeneration temperatures: 320, 350, 380, and 450°C, and (b) the relative C and S removals after 64 minutes. Full symbol regeneration carried out in the NTP reactor (turn-off) (**TR<sub>DBD</sub> reactor**) , open symbol: regeneration at the lab scale (**O-TR**),

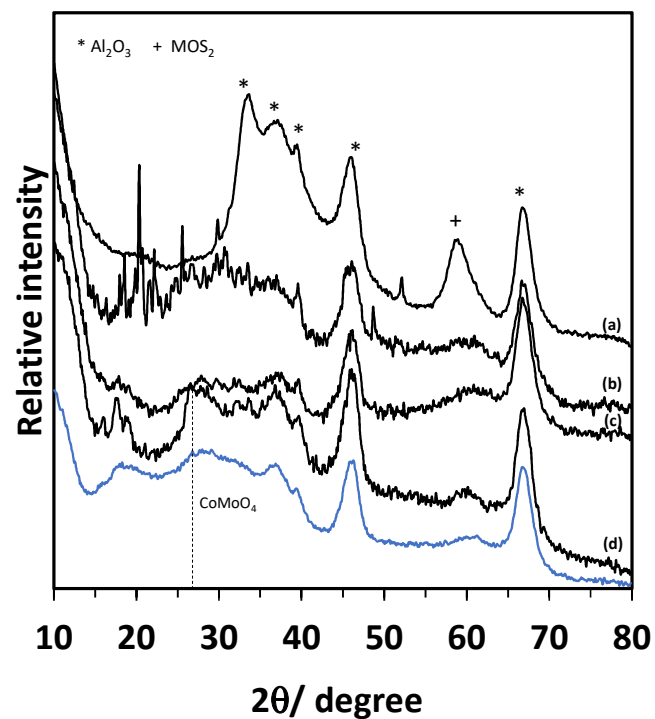


**Figure 4:** XRD patterns of spent catalyst before (a) and after thermal regeneration during 30 min at 200 (b), 300 (c) and 500°C (d). in blue after plasma treatment at 200°C with 7W

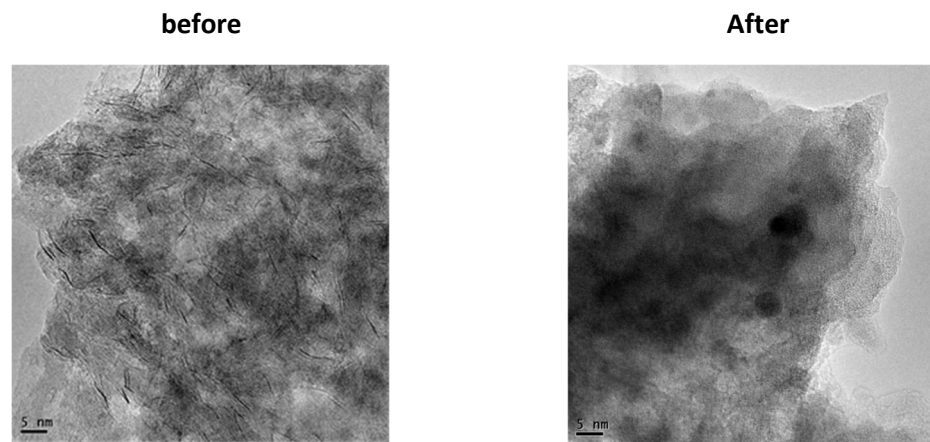


**Figure 5:** TEM images of spent catalyst before after thermal regeneration during 30mins at 500 °C

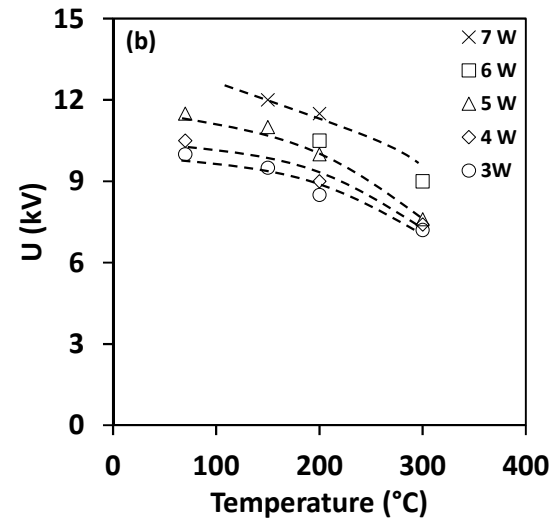
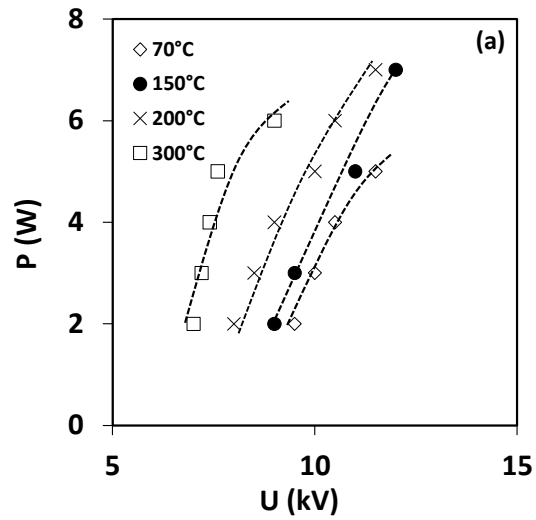


**Figure 6:** Impact of temperature on deposited power ( $P$ ): **(a)**  $P$  at different temperatures: 70, 150, 200 and 300°C as a function of the applied voltage; **(b)** Applied voltage ( $U$ ) required to obtain a deposited power of 3, 4, 5, 6 and 7W as a function of the temperature

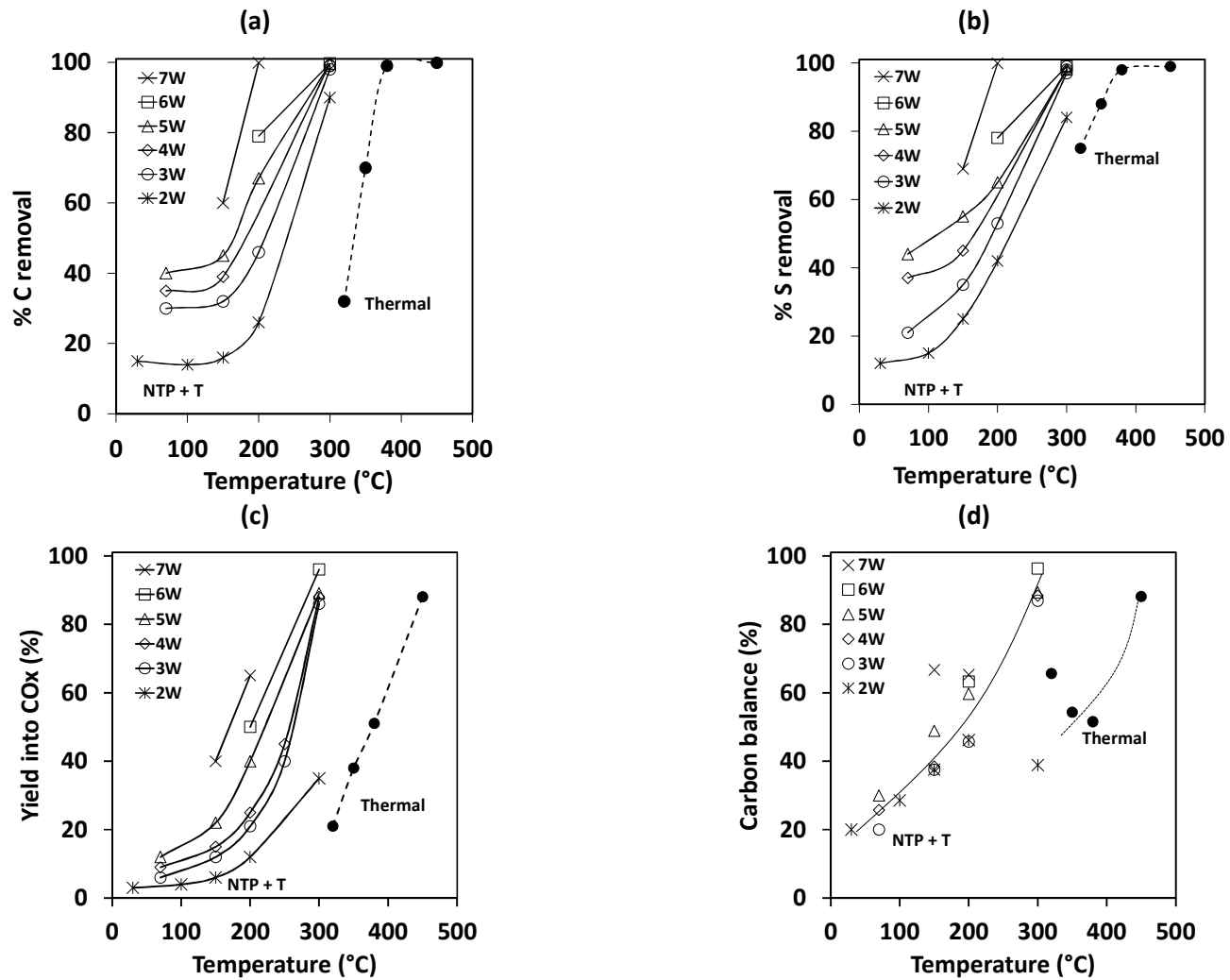


**Figure 7:** Impact of temperature on the efficiency of non-thermal plasma on: (a,b) carbon and sulfur removal, (c) cumulated conversion to CO<sub>x</sub> (CO<sub>2</sub>+CO), (d) carbon balance and comparison with thermal regeneration (Full symbol). Results obtained after 1h regeneration at different applied powers (2, 3, 4, 5, 6 and 7W);

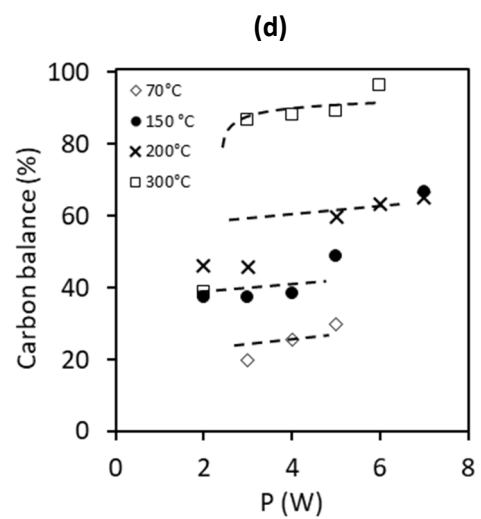
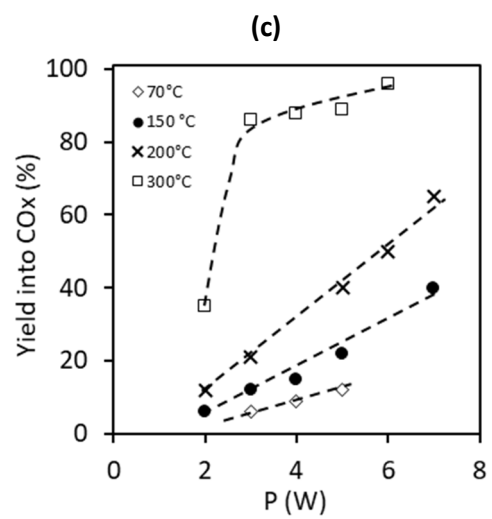
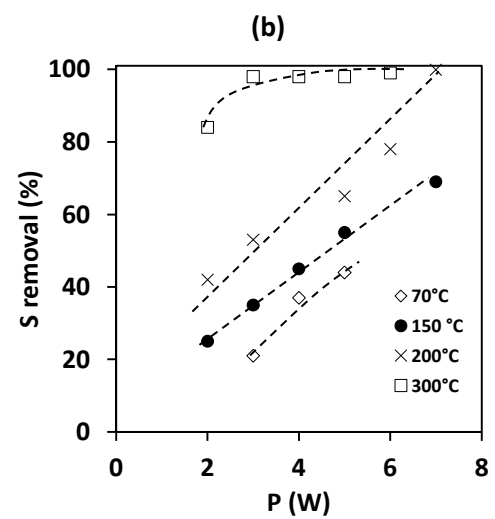
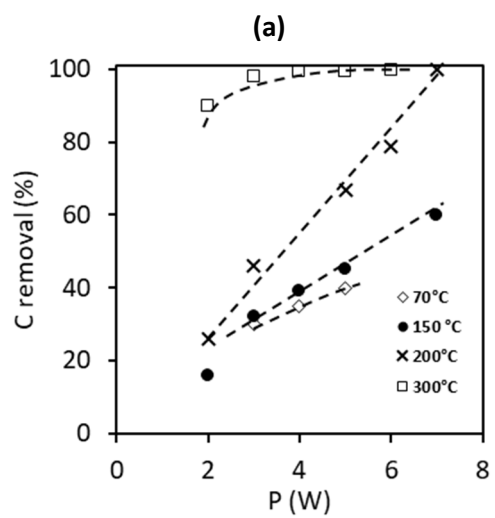


**Figure 8:** Impact of applied power (P) on the efficiency of NTP on (a,b) carbon and sulfur removal, (c) cumulated conversion to CO<sub>x</sub> (CO<sub>2</sub>+CO), (d) carbon balance. Results obtained after 1h regeneration at different temperatures: 70, 150, 200 and 300°C.

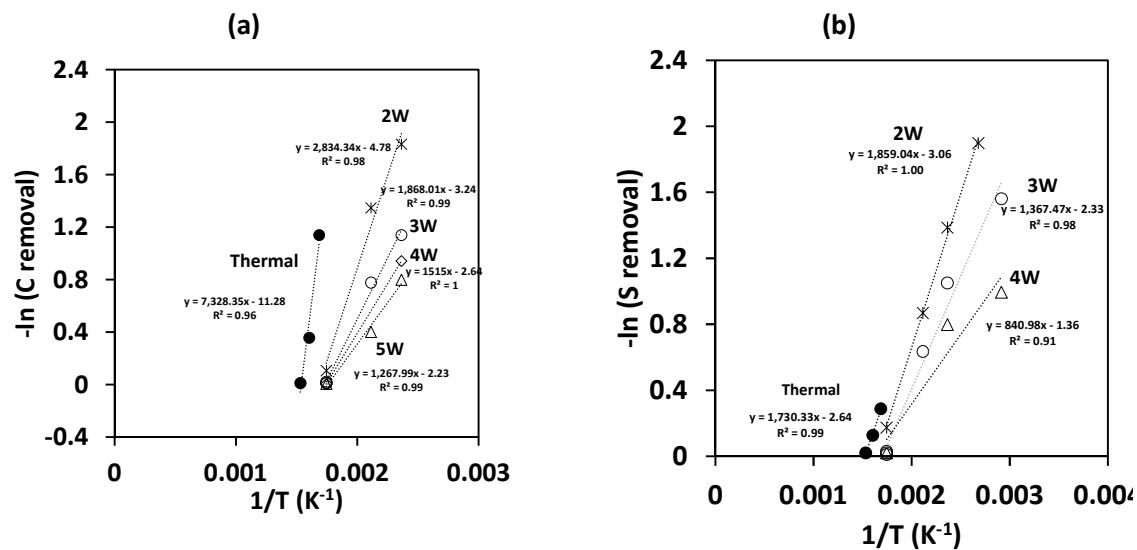


**Figure 9:** Temperature dependency of removal of carbon (a) and sulfur (b) as a function of the applied power. Results obtained after 1h regeneration

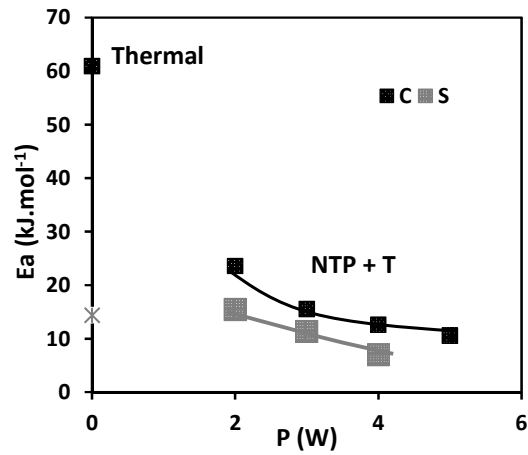


**Figure 10:** Apparent activation energy ( $E_a$ ) as a function of the applied power. Results obtained after 1h regeneration

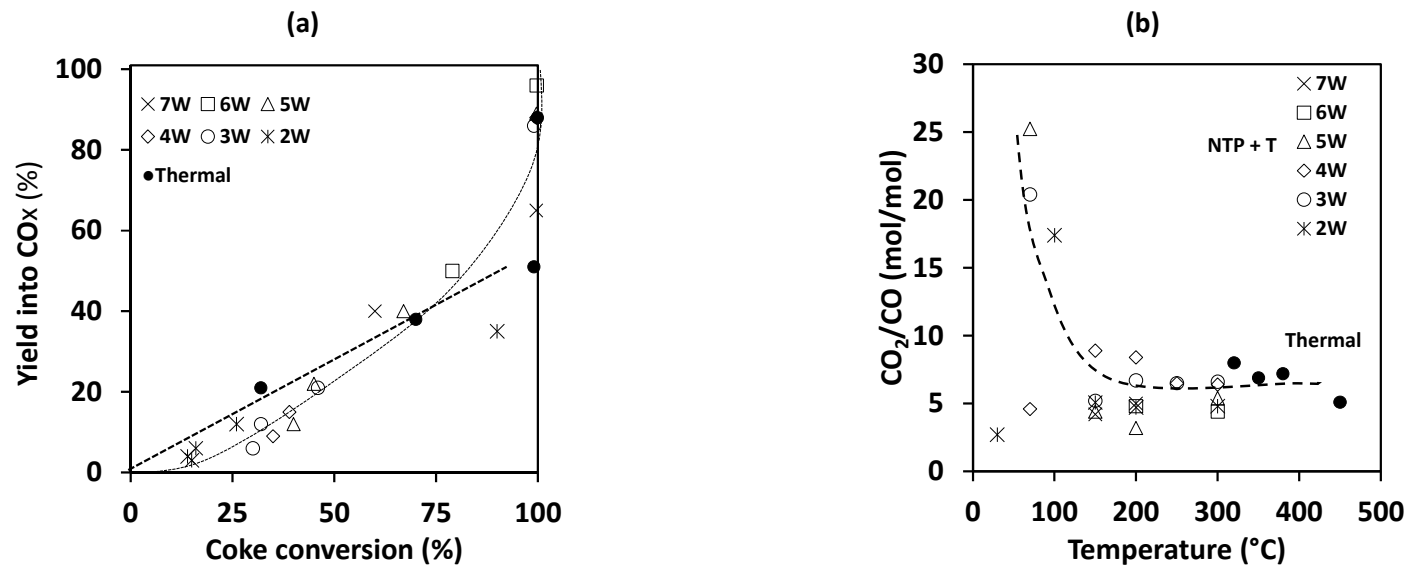


**Figure 11:** Selectivity of NTP process:  
**(a)** Cumulated yield into CO<sub>x</sub> after 1h as a function of coke conversion drawn from elementary analysis,  
**(b)** Molar ratio of CO<sub>2</sub>/CO at different applied power as a function of temperature

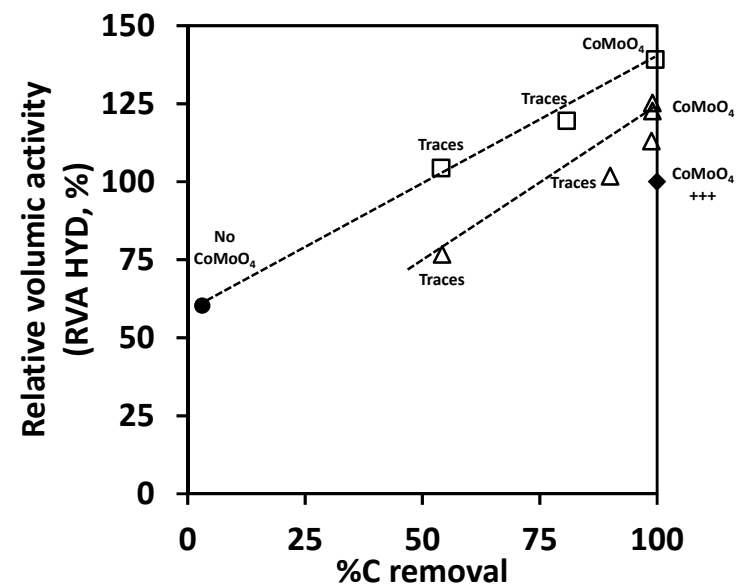


**Figure 12:** Relative Volumic Activity of toluene hydrogenation (the industrial regenerated catalyst activity being the reference) of spent catalyst (●) and regenerated catalysts by IT-R (♦), OTR (□) and NTP-R (Δ) processes.

